JOURNAL OF GUIDANCE, CONTROL, AND DYNAMICS
Vol. 30, No. 5, September–October 2007

Head Pursuit Guidance

Tal Shima*
Technion—Israel Institute of Technology, 32000 Haifa, Israel
and
Oded M. Golan†
RAFAEL, 31021 Haifa, Israel

DOI: 10.2514/1.27737

A guidance law for intercepting high-speed targets in a novel head pursuit engagement is presented. The guidance law imposes a geometric relation in which the interceptor missile is positioned ahead of the target so that both fly in the same direction. The missile speed is planned to be lower than that of the target, and therefore the target closes in on the interceptor missile and it is intercepted from its front end. The guidance law also enables enforcing a predetermined interception angle relative to the target's flight direction. Analytic conditions enabling interception in this novel engagement are provided. The guidance law is implemented using the sliding mode approach, and simulation results confirm its viability in several representative engagements against maneuvering high-speed targets.

I. Introduction

INTERCEPTION of high-speed targets, such as reentering ballistic missiles, is a formidable challenge. The interception in these scenarios is typically head-on, with a very high closing speed. This imposes severe requirements on the interceptor systems such as precise detection of the target from a large distance by the onboard seekers, and very fast response time of the missile subsystems. To overcome these difficulties, a different approach was suggested in [1], in which the interceptor velocity is matched with that of the target by a preliminary maneuver. If the target path is predictable, as in the case of ballistic missiles, the maneuver can be designed such that the interceptor missile is positioned ahead of the target on its predicted flight path, flying in the same direction but at a slightly lower speed. This way the target closes in on the interceptor that is conducting the necessary lateral maneuvers to achieve interception. The interceptor speed along the target's predicted path can be selected to achieve a desired closing rate. A similar low closing speed can be obtained in a tail-chase scenario. However, tail chase requires that the interceptor will be faster than the target, and therefore more energy is needed during the preliminary maneuver to reach the desired closing speed.

Various guidance methods have been examined for implementation in the different stages of high-speed exo- or endo-atmospheric interception scenarios of ballistic missiles. Some of these methods are described next. In [2] a modified version of proportional navigation (PN) guidance law [3] was proposed for implementation in the coast phase. A variable bias was applied to the actual line of sight (LOS) to account for engine burn. The terminal guidance in a hyper-velocity exo-atmospheric orbital interception was studied in [4]. The control energy expenditure is reduced by constraining the expected final state to a function of the estimation error. An optimal guidance algorithm was proposed in [5] for the interception of a nonmaneuvering target decelerated by atmospheric drag. Its implementation requires knowledge on many scenario states, obtained from a nonlinear state estimator. In a recent paper [6] a differential game guidance law was proposed against targets having known speed and lateral acceleration limit profiles. It was shown that in a ballistic missile interception scenario such a guidance law provides a significant improvement in the homing accuracy compared to a guidance law derived based on a model with constant speeds and lateral acceleration limits. Although all of the aforementioned guidance laws may provide interception in some scenarios, the actual geometry of the engagement is not imposed. It is a result of the specific initial conditions, target maneuvers, and guidance law used.

The simple guidance law of pure pursuit (PP) and its derivative deviated PP (DPP) [7] can impose a final interception geometry. In PP the interceptor is aimed at the target and it is intercepted from its rear [8]. The DPP guidance law is an extension of PP in that the missile is aimed at a constant lead angle to the target and the target is intercepted from a constant angle, dependent on the lead angle and speed ratio [7]. Such guidance laws require minimal knowledge of the interception state variables and future target maneuvers. However, they impose severe maneuver requirements and necessitate a velocity advantage of the interceptor. Imposing an impact angle can also be performed by a circular navigation guidance law [9]. The name of this guidance law stems from the imposed approach path along an arc of a circle towards the target. A more complicated guidance law that can impose initial and final flight-path angles was introduced in [10]. The algorithm requires the solution of a two-point boundary value problem and thus can be implemented against targets with known trajectories.

Imposing the impact angle alone will not enable following the unique geometry outlined in [1]. It is also needed that the target's head will be hit while the interceptor has a speed disadvantage. In a recent paper by the authors [11] it was shown that by maintaining a simple geometric rule, the trajectory proposed in [1] can be achieved. The term head pursuit (HP) was coined to indicate that interception is aimed at always hitting the target's head. It was also shown that imposing this geometric rule is equivalent to being in sliding mode.

The sliding mode control (SMC) methodology is a well-known method described in many papers and textbooks [12–14]. It is a robust control technique, addressing highly nonlinear systems with large modeling errors and uncertainties. In SMC the controller is obtained by converting an nth-order tracking problem to a first-order stabilization problem. The design is performed around a sliding surface commonly denoted by $\sigma = 0$, where the sliding variable σ is a function of the system tracking error and possibly its derivatives. The problem is to drive the scalar quantity defining the sliding surface to zero, and maintain it there, ultimately achieving exact tracking. When the system response is confined to the sliding surface, it is said that the system is in a sliding mode.

Received 20 September 2006; revision received 25 January 2007; accepted for publication 16 February 2007.

*Senior Lecturer, Department of Aerospace Engineering; tal.shima@technion.ac.il. Senior Member AIAA.

†Systems Engineer, P.O. Box 2250, Department M5; odedgol@rafael.co.il. Senior Member AIAA.

The SMC methodology has been successfully used in various guidance applications. A missile guidance law in the class of PN, derived using the SMC approach, was proposed in [15]. The sliding surface was selected to be proportional to the LOS rate and the target maneuvers were considered as bounded uncertainties. Using numerical simulations, the superiority of the proposed guidance law over the conventional PN was advocated. In [16] an adaptive sliding mode guidance law was derived. Using analysis and simulations, robustness to disturbances and parameter perturbations was shown.

In this paper we develop a guidance law for the unique HP engagement. In the next section, the interception engagement is outlined and a guidance law is proposed. Analytic conditions for providing interception in an ideal scenario, with no missile maneuver dynamics and bounds, are given next. A sliding mode controller is then developed and its performance is examined through simulation. Concluding remarks are offered in the last section.

II. Head Pursuit Interception

A. Engagement

The schematic view of the proposed engagement is shown in Fig. 1. In the beginning of the endgame phase, the interceptor is flying in the same general direction as the target, but ahead of it at a lower speed. In this unconventional final geometry, the target approaches the interceptor from its rear end. Using this approach the closing speed is significantly reduced relative to a head-on engagement; compared to a tail-chase engagement, the low closing speed is achieved with reduced energy requirements. In an endo-atmospheric interception, such geometry also relaxes the requirements from the interceptor seeker dome because it is not exposed to the high aerodynamic heating (as the seeker is pointed away from the interceptor's flight direction). However, in contrast to the general trend in new interceptors to achieve lethality by direct hit, in a HP interception a kill mechanism, such as fragmentation warhead, is required (because the closing speed is small).

A perfect information scenario, with no measurement noise, is analyzed in this paper. We assume that the interceptor is roll controlled and thus for the relatively short time interval of the endgame (with small changes in the flight direction) the motion of such an interceptor can be separated into two perpendicular channels and the guidance problem can be treated as planar in each of these channels. The planar endgame geometry is shown in Fig. 2. The target T is located behind the slower interceptor I. The speed, maneuvering acceleration, and flight-path angle are denoted by V, a, and γ, respectively; the range between the target and interceptor is r, and λ is the LOS angle relative to a fixed reference. The angles θ and δ are the instantaneous target and interceptor direction of flight relative to the LOS.

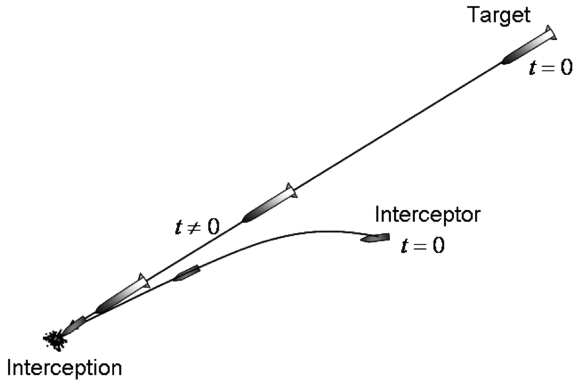

Fig. 1 Endgame HP engagement.

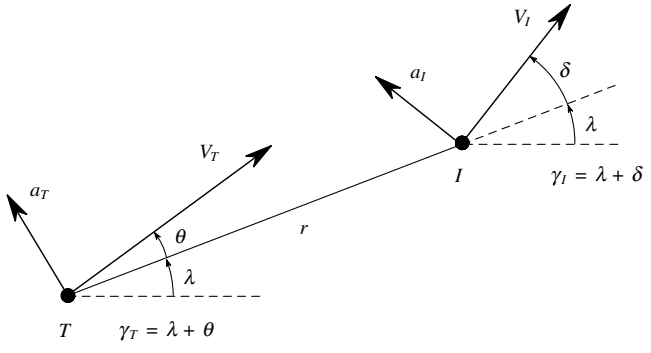

Fig. 2 Planar engagement geometry.

B. Kinematics

The engagement kinematics is expressed in a polar coordinate system (r, λ) attached to the target

$$\dot{r} = V_r \tag{1a}$$

$$\dot{\lambda} = V_\lambda / r \tag{1b}$$

where the speed V_r is

$$V_r = V_I \cos\delta - V_T \cos\theta \tag{2}$$

and the speed perpendicular to the LOS is

$$V_\lambda = V_I \sin\delta - V_T \sin\theta \tag{3}$$

A scenario in which the interceptor is designed with a speed disadvantage is analyzed. We assume that the interceptor and target speeds, V_I and V_T, are constant and define the nondimensional parameter K as the speed ratio

$$K \triangleq V_I / V_T < 1 \tag{4}$$

The lateral accelerations a_I and a_T determine the interceptor and target trajectories

$$\dot{\gamma}_I = a_I / V_I \tag{5a}$$

$$\dot{\gamma}_T = a_T / V_T \tag{5b}$$

where the flight-path angles γ_I and γ_T satisfy

$$\gamma_I = \lambda + \delta \tag{6a}$$

$$\gamma_T = \lambda + \theta \tag{6b}$$

From Eqs. (5) and (6) we obtain

$$\dot{\delta} = a_I / V_I - V_\lambda / r \tag{7a}$$

$$\dot{\theta} = a_T / V_T - V_\lambda / r \tag{7b}$$

C. Guidance Law

We denote the running time as t. The endgame initiates at $t = 0$ with $\dot{r}(t = 0) < 0$ and terminates at $t = t_f$ where

$$t_f = \arg\{r(t)\dot{r}(t) = 0\} \tag{8}$$

The miss distance is $r(t_f)$.

Using the preceding notations, we make the following definitions:

Definition 1: Head pursuit. An interception engagement where $K < 1$, $|\theta(t_f^-)| < \pi/2$, and $|\delta(t_f^-)| < \pi/2$.

Definition 2: Perfect head pursuit. HP where $\theta(t_f^-) = 0$; and consequently $r(t_f) = 0$.

The objective of a guidance law for HP can be to impose

$$\theta(t_f^-) = \theta_r \tag{9}$$

where $|\theta_r| < \pi/2$ is selected by the designer.

For obtaining a guidance law enabling HP, we propose maintaining the interceptor's lead angle proportional to the error from the target's required flight direction relative to the LOS. This geometric rule is

$$\delta - \delta_r = n(\theta - \theta_r) \tag{10}$$

where

$$\delta_r = \sin^{-1}[\sin(\theta_r)/K]; \qquad |\delta_r| < \pi/2 \tag{11}$$

and n is the guidance constant. Using this rule, for $\theta = \theta_r$ we obtain $\delta = \delta_r$ and, from Eq. (3), the LOS does not rotate. For perfect HP the geometric rule of Eq. (10) degenerates to

$$\delta = n\theta \tag{12}$$

III. Ideal Head Pursuit

In this section we address analytically an ideal HP with no interceptor maneuver dynamics and acceleration bounds. The relationship between the guidance constant n, the interceptor/target speed ratio K, and the initial conditions, is studied.

A. Interception Conditions

Theorem 1: Against a nonmaneuvering target, a necessary condition to achieve HP with $\theta(t_f^-) = \theta_r$, where $\text{sgn}\theta(0) = \text{sgn}\theta_r$ and $|\theta(0)| > |\theta_r|$, is

$$|\theta(t)| < \theta_{\max} \tag{13}$$

where $\theta_{\max}$ is defined as

$$\theta_{\max} = \sin^{-1}(K); \qquad 0 < K < 1 \tag{14}$$

Proof: If $\theta(t) \geq \theta_{\max}$ then $\dot{\theta}(t) \geq 0$ from t to t_f and thus $\theta(t_f^-) = \theta_r$ cannot be reached. For $\theta(t) < 0$ the condition is proved by symmetry. □

From Theorem 1 it follows that $|\theta_r| < \sin^{-1}(K)$ should be selected.

Theorem 2: Against a target performing a constant maneuver a_T^{const}, a necessary condition for HP with $\theta(t_f^-) = \theta_r$, where $\text{sign}(a_T^{\text{const}}) = \text{sign}[\theta(0)]$ and $|\theta(0)| > |\theta_r|$, is

$$|\theta(t)| < \theta_{\max}^a \quad \forall\ t \in [t_1, t_f), \qquad t_1 \geq 0 \tag{15}$$

where

$$\theta_{\max}^a = \sin^{-1}[K - |a_T^{\text{const}}|r(t)/V_T^2]; \qquad |a_T^{\text{const}}|r(t)/V_T^2 < K < 1 \tag{16}$$

Proof: On the final interval $[t_1, t_f)$ for $a_T^{\text{const}} > 0$ and $\theta(t) > 0$, if $\theta(t) \geq \theta_{\max}^a$ then $\dot{\theta} \geq 0$ from t_1 to t_f and consequently the end condition $\theta(t_f^-) = \theta_r$ cannot be enforced. For $\theta(t) < 0$ the condition is proved by symmetry. □

From Eq. (15) it is apparent that, as expected, the limit on the angle θ is proportional to the target's maneuver and the range, while being inversely proportional to the target's speed. The relationships of Eqs. (13) and (15) are plotted in Fig. 3, in which the feasible target direction of flight relative to the LOS lies under the respective curves. Because of symmetry the results are plotted only for $\theta > 0$.

Theorem 3: Against a nonmaneuvering target with $\theta(0) \neq 0$, a necessary condition for perfect HP, maintaining the geometric rule of Eq. (12), is

$$n > 1/K \tag{17}$$

Proof: The path angle γ_T, of the nonmaneuvering target, is constant and hence $\dot{\lambda} = -\dot{\theta}$. For perfect HP the following relation must hold at $r \to 0$:

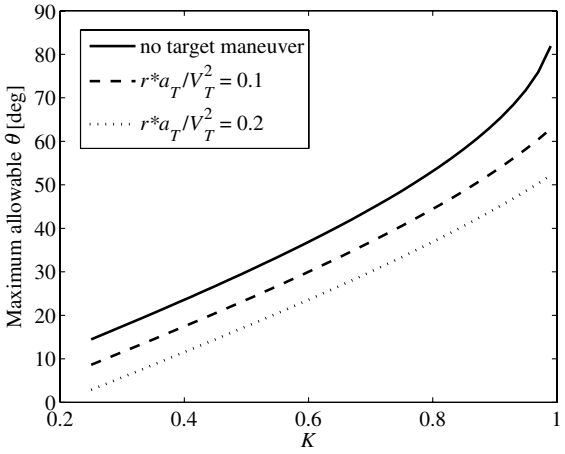

Fig. 3 Maximum allowable target heading relative to LOS.

$$\text{sgn}(\theta) = -\text{sgn}(\dot{\theta}); \qquad \theta \neq 0 \tag{18}$$

and the angles δ and θ should be small. Therefore, from Eq. (1) we obtain

$$\dot{\lambda} \approx V_T(Kn - 1)\theta/r \tag{19}$$

and using the relationship $\dot{\lambda} = -\dot{\theta}$

$$\dot{\theta} \approx -V_T(Kn - 1)\theta/r \tag{20}$$

Using Eq. (20), for Eq. (18) to hold, the relationship given in Eq. (17) must be satisfied and the theorem is proved. □

We define θ_m as the solution of

$$\theta_m(n, K) = \arg_{\theta}[\dot{\theta}|_{a_T=0} = -V_T(K\sin\delta - \sin\theta)/r = 0]; \quad 0 < \theta < \pi/2 \tag{21}$$

with $\delta = n\theta$. For specific values of n an exact solution of Eq. (21) exists. For example for $n = 2$ the condition is

$$\theta_m(2, K) = \cos^{-1}(1/2K) \tag{22}$$

and for $n = 3$ it is

$$\theta_m(3, K) = \sin^{-1}\text{sqrt}[(3K - 1)/4K] \tag{23}$$

Theorem 4: Against a nonmaneuvering target, a sufficient condition for performing perfect HP, maintaining the geometric rule of Eq. (12) and given $n > 1/K$, is

$$|\theta(0)| < \theta_m(n, K) \tag{24}$$

Proof: By the relationship $\dot{\lambda} = -\dot{\theta}$ and Eqs. (1) and (12)

$$\dot{\theta} = -V_T(K\sin n\theta - \sin\theta)/r \tag{25}$$

If $|\theta(0)| < \theta_m$ then $\text{sgn}[\dot{\theta}(t)] = -\text{sgn}[\theta(t)] \quad \forall\ t \in [0, t_f)$. Because $\dot{\theta}$ is inversely proportional to r, then as r decreases $|\dot{\theta}|$ increases and $\dot{\theta}$ vanishes only when $\theta \to 0$. □

In Fig. 4 θ_m is plotted for different values of n and K. Note that for every speed ratio K there is an optimal value of n that guarantees a maximum angle of θ_m, which is $\theta_{\max}$ defined in Eq. (14), where

$$\theta_{\max} = \theta_m(n_{\max}, K); \qquad 0 < K < 1 \tag{26}$$

and

$$n_{\max} = \arg_n\{\max[\theta_m(n, K)]\}; \qquad 0 < K < 1 \tag{27}$$

Note that $\theta_{\max} n_{\max} = \pi/2$ as these values are obtained when the interceptor's velocity is perpendicular to the LOS. The relationship

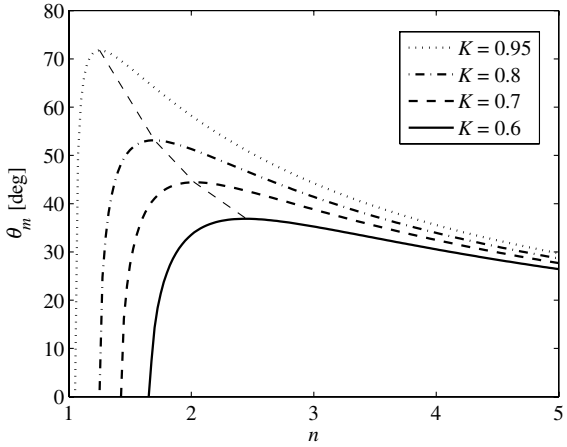

Fig. 4 Conditions for perfect HP.

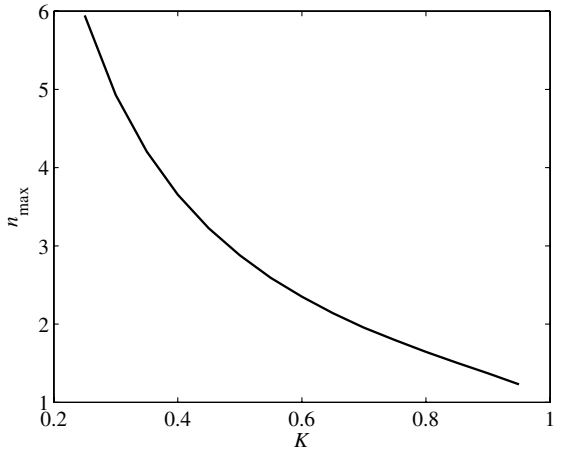

Fig. 5 Optimal value of *n* for largest perfect HP interception envelope.

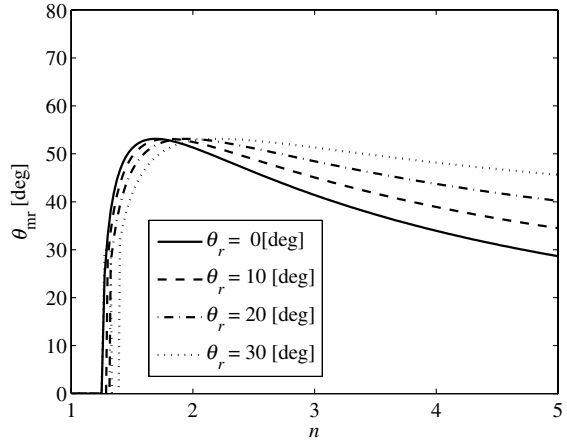

Fig. 6 Conditions for HP; $K = 0.8$.

from Eq. (27) is plotted in Fig. 5. From Fig. 4 it is evident that given K, for $\theta_m < \theta_{\max}$ there exists a solution of Eq. (21) for two values of n denoted n_1, n_2 and let $n_1 < n_2$. This suggests that if $\theta(0) = \theta_m(n_1, K) = \theta_m(n_2, K)$ and $n_1 < n < n_2$ then HP is achieved. Interestingly, if $n_{\max} < n < n_2$ then the scenario starts as head-on and turns later to HP; whereas for $n_1 < n < n_{\max}$ it is HP for the entire duration.

Figure 6 presents the solution of

$$\theta_{mr} = \arg_{\theta}[\dot{\theta}|_{a_T=0} = V_T(K\sin\delta - \sin\theta)/r = 0] \tag{28}$$

with $\delta = n(\theta - \theta_r) + \delta_r$ obtained from Eq. (10). The results are plotted for HP with different requirements on θ_r, the final required target direction of flight relative to the LOS. As expected the maximum value of θ_{mr} is independent on the value of θ_r as it is dependent only on the capabilities of the adversaries to rotate the LOS, and hence on K alone. Note that the optimal value of n providing this maximum is dependent on θ_r.

B. HP Analytic Trajectories

For a nonmaneuvering target, the equations of motion can be solved in the polar (r, λ) coordinates. From Eq. (1) we obtain

$$\frac{\mathrm{d}r}{\mathrm{d}\lambda} = \frac{V_I\cos\delta - V_T\cos\theta}{V_I\sin\delta - V_T\sin\theta}r \tag{29}$$

Substituting the perfect HP geometric rule $\delta = n\theta$ of Eq. (12) and rearranging

$$\frac{\mathrm{d}r}{r} = f(\theta)\,\mathrm{d}\lambda \tag{30}$$

where

$$f(\theta) = \frac{K\cos n\theta - \cos\theta}{K\sin n\theta - \sin\theta} \tag{31}$$

Using the relationship $\gamma_T = \theta + \lambda$, and because for a nonmaneuvering target $\gamma_T = \text{const}$, we can write

$$\frac{\mathrm{d}r}{r} = -f(\theta)\,\mathrm{d}\theta \tag{32}$$

By direct integration of Eq. (32), we obtain

$$\frac{r}{r(0)} = \exp[g(\theta)] \tag{33}$$

where

$$g \equiv -\int_{\theta(0)}^{\theta} f(\ni)\,\mathrm{d}\ni \tag{34}$$

For some values of n, an analytical solution of Eq. (34) can be obtained. For example, for $n = 2$ the solution is

$$g(\theta) = \ell_n\frac{\psi^2+1}{\psi_0^2+1} - \frac{K-1}{2K-1}\ell_n\frac{\psi}{\psi_0} - \frac{2K^2}{4K^2-1}\ell_n\frac{(2K+1)\psi^2-(2K-1)}{(2K+1)\psi_0^2-(2K-1)} \tag{35}$$

and for $n = 3$ it is

$$g(\theta) = \ell_n\frac{\psi^2+1}{\psi_0^2+1} - \frac{K-1}{3K-1}\ell_n\frac{\psi}{\psi_0} - \frac{K}{3K-1}\ell_n\frac{(3K-1)\psi^4-2(5K+1)\psi^2+3K-1}{(3K-1)\psi_0^4-2(5K+1)\psi_0^2+3K-1} \tag{36}$$

where

$$\psi \equiv \tan(\theta/2) \tag{37}$$

and $\psi_0 \equiv \tan[\theta(0)/2]$.

Similarly, using the HP geometric rule $\delta = \delta_r + n(\theta - \theta_r)$, an analytic solution of Eq. (29) for $\theta_r \neq 0$ can be obtained. The solution for $n = 3$ and $\theta_r = \pi/6$ is

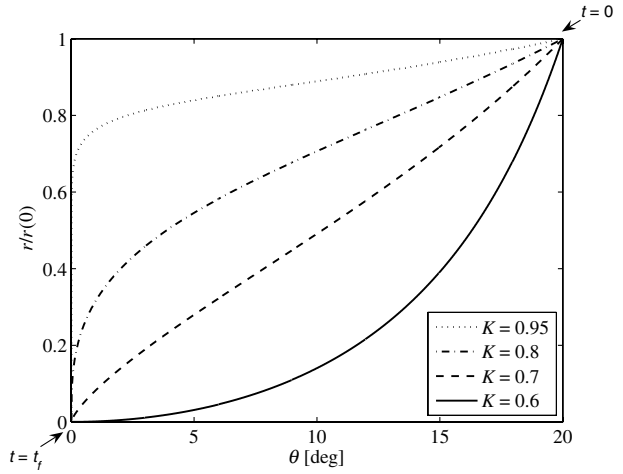

Fig. 7 Perfect HP trajectories in target coordinate system; $n = 2$ and $\theta(0) = 20$ deg.

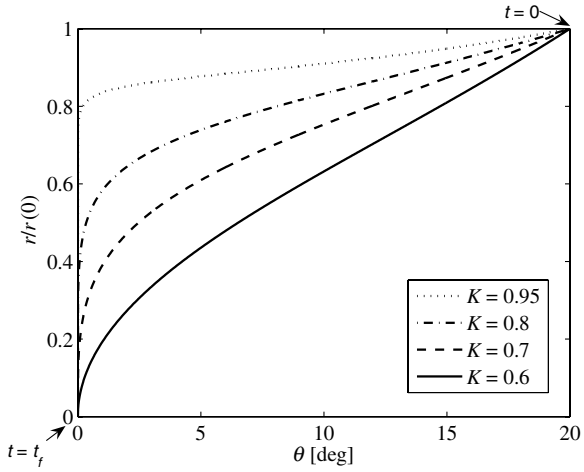

Fig. 9 Perfect HP trajectories in target coordinate system; $n = 3$ and $\theta(0) = 20$ deg.

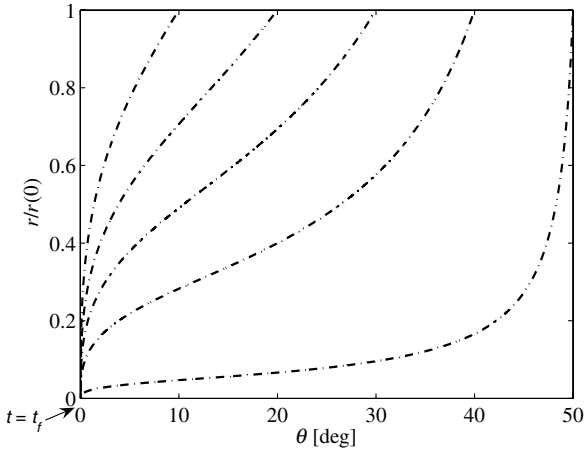

Fig. 8 Perfect HP trajectories in target coordinate system; $n = 2$, $K = 0.8$.

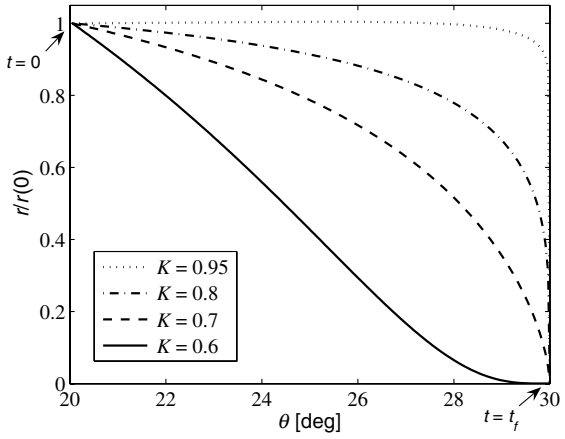

Fig. 10 HP trajectories in target coordinate system; $n = 3$, $\theta(0) = 20$ deg, and $\theta_r = 30$ deg.

$$g(\theta) = \ell_n \frac{\psi^2+1}{\psi_0^2+1} - \frac{2K^2-1}{2(3K^2-1)} \ell_n \frac{(\psi^2+1)^2 - 16\psi^2}{(\psi_0^2+1)^2 - 16\psi_0^2} + \frac{\sqrt{4K^2-1}}{2\sqrt{3}(3K^2-1)} \ell_n \frac{(\psi^2+2\sqrt{3}\psi-1)(\psi_0^2-2\sqrt{3}\psi_0-1)}{(\psi^2-2\sqrt{3}\psi-1)(\psi_0^2+2\sqrt{3}\psi_0-1)} - \frac{K^2}{3K^2-1} \ell_n \frac{\psi^2+2/\sqrt{4K^2-1}\psi-1}{\psi_0^2+2/\sqrt{4K^2-1}\psi_0-1} \tag{38}$$

Solutions of Eq. (33) are shown in Fig. 7, for $n = 2$. The plot shows the trajectories obtained for different values of K and an initial condition of $\theta(0) = 20$ deg, maintaining $|\theta(0)| < \sin^{-1}(K)$ from Eq. (13). It can be observed that near the limiting case of $nK \to 1$, when $K = 0.6$, interception is achieved but the required directional condition of $\theta(t_f^-) = 0$ is achieved only close to interception. As the speed ratio is increased (i.e., the interceptor's speed is closer to that of the target), the easier it becomes for the interceptor to position itself ahead of the target and reach the desired interception condition. In Fig. 8 the trajectories are plotted from different initial condition $\theta(0)$, for $n = 2$ and $K = 0.8$. Obviously, a smaller initial deviation from the required end condition of $\theta(t_f^-) = 0$ deg enables an earlier convergence to this value. Note that similar trajectories exist up to the limiting case of $\theta(0) \approx 51.3$ deg obtained as the solution of Eq. (14) for $K = 0.8$.

Similar to Fig. 7, in Fig. 9 solutions of Eq. (33) are shown, but for $n = 3$. Comparing these two figures reveals that a larger value of n causes the trajectories to approach the required end condition earlier on.

Figure 10 presents the solution of Eq. (29) with $n = 3$, but for $\theta_r = 30$ deg. Note that for $K = 0.95$, that is, when the adversaries have similar speeds, the range is initially increased. This is due to the fact that starting with $\theta(0) = 20$ deg $< \theta_r$ the interceptor's initial heading angle relative to the LOS (δ) is small, resulting in a small negative closing speed.

IV. Implementing Head Pursuit Guidance

In this section a guidance law is derived for HP with modeling errors and target maneuvers. The derivation is performed using the sliding mode approach. Next, we present the adversaries dynamics, define the sliding variable, and then derive the sliding mode HP controller.

A. Dynamics

We assume that both the interceptor and target closed-loop lateral acceleration dynamics can be represented by equivalent first-order transfer functions:

$$\dot{a_I} = (a_I^c - a_I)/\tau_I + \Delta_I \tag{39}$$

$$\dot{a_T} = (a_T^c - a_T)/\tau_T + \Delta_T \tag{40}$$

where τ_I and τ_T are the respective interceptor and target time constants, and Δ_I, Δ_T are their bounded modeling errors:

$$|\Delta_I| \le \bar{\Delta}_I \tag{41}$$

$$|\Delta_T| \le \bar{\Delta}_T \tag{42}$$

In aerodynamically controlled vehicles, these dynamics represent the closed-loop response of the missile airframe to the commands.

We also assume that the target's acceleration command is bounded:

$$|a_T^c| \le a_T^{\max} \tag{43}$$

B. Sliding Variable

We define the deviation from the geometric rule of Eq. (10) as

$$e = \delta - \delta_r - n(\theta - \theta_r) \tag{44}$$

The relative degree of this error is two as the second derivative of e yields the maneuver command a_I^c. Consequently, the sliding variable should include a first derivative of the error e. This will guarantee that the control will have direct effect on the sliding surface. Thus, the SMC sliding variable is defined as

$$\sigma = e + \tau\dot{e} \tag{45}$$

The time constant τ can be selected such that the error e diminishes to zero at the required rate, regardless of the value of the control. Substituting Eqs. (5), (6), and (44) in Eq. (45) we can write the sliding variable as

$$\sigma = \gamma_I - n\gamma_T + (n-1)\lambda + \tau[a_I/V_I - na_T/V_T + (n-1)V_\lambda/r] + n\theta_r - \delta_r \tag{46}$$

Differentiating Eq. (46) yields the dynamics of this sliding variable:

$$\dot{\sigma} = a_I/V_I - na_T/V_T + (n-1)V_\lambda/r + \tau[(a_I^c - a_I)/\tau_I/V_I + \Delta_I/V_I - n(a_T^c - a_T)/\tau_T/V_T - n\Delta_T/V_T] + \tau(n-1)(\dot{V}_\lambda r - V_\lambda V_r)/r^2 \tag{47}$$

where V_r and V_λ are given in Eqs. (2) and (3) and

$$\dot{V}_\lambda = a_I \cos\delta - a_T \cos\theta - V_\lambda V_r/r \tag{48}$$

C. Sliding Mode Controller

The sliding mode controller a_I^c consists of an equivalent part denoted $a_{I\text{eq}}^c$ and an uncertainty part denoted $a_{I\text{uc}}^c$:

$$a_I^c = a_{I\text{eq}}^c + a_{I\text{uc}}^c \tag{49}$$

The equivalent controller is designed to maintain the system on the sliding surface, by imposing $\dot{\sigma} = 0$, in the absence of modeling errors and target maneuver commands. Thus, from Eq. (47) with $\Delta_{(\cdot)} = 0$ and $a_T^c = 0$, we obtain

$$a_{I\text{eq}}^c = f_I a_I + f_T a_T + f_\lambda \dot{\lambda} \tag{50}$$

where

$$f_I = 1 - \tau_I/\tau - \tau_I(n-1)V_I \cos\delta/r \tag{51}$$

$$f_T = Kn(\tau_I/\tau - \tau_I/\tau_T) + V_I(n-1)\tau_I \cos\theta/r \tag{52}$$

$$f_\lambda = V_I\tau_I(n-1)(2V_r/r - 1/\tau) \tag{53}$$

Modeling errors and target maneuvers will cause the system to depart from the sliding surface. The uncertainty controller is designed to drive the system to the sliding surface in finite time in the face of these errors and uncertainties. Here, the design of the uncertainty controller is based on the model of the interceptor and target dynamics and the bounds given in Eqs. (39–43). We select the uncertainty controller in the form

$$a_{I\text{uc}}^c = \tau_I V_I \mu \,\text{sign}(\sigma) \tag{54}$$

The gain μ is obtained from the following stability analysis: We select the Lyapunov function

$$\mathcal{L} = \sigma^2/2 \tag{55}$$

Using the time derivative of this function, the reaching condition is obtained:

$$\dot{\mathcal{L}} = \sigma\dot{\sigma} < 0 \tag{56}$$

This derivative with the equivalent and uncertainty controllers of Eqs. (50) and (54), is

$$\dot{\mathcal{L}} = \sigma\dot{\sigma} = \tau\sigma[\mu \,\text{sign}(\sigma) + \Delta_I/V_I - n\Delta_T/V_T - na_T^c] \tag{57}$$

Using the bounds from Eqs. (41–43), this derivative can be bounded by

$$\dot{\mathcal{L}} \le \tau|\sigma|[\mu + \bar{\Delta}_I/V_I + n\bar{\Delta}_T/V_T + na_T^{\max}] \tag{58}$$

To obtain finite time convergence to the sliding surface, we choose

$$\mu < -[\bar{\Delta}_I/V_I + n\bar{\Delta}_T/V_T + na_T^{\max}] \tag{59}$$

such that negative definiteness of the Lyapunov function is ensured. Note that to avoid chattering, as a result of the discontinuous command in Eqs. (54), a boundary-layer approximation of the sign function can be used, thus compromising exact tracking by uniform ultimate boundedness of the tracking error [12].

Remark: The gain μ is proportional to n. To obtain the largest interception envelope, n should be chosen based on the results plotted, for example, in Figs. 4–6. Nonetheless, it should not be chosen too large so that the interceptor's maneuver capability will not be exceeded.

V. Performance Analysis

In this section perfect information HP is studied using planar nonlinear simulations. The simulation parameters are summarized in Table 1. To avoid excessive chattering, the guidance law was implemented with a boundary layer around the sliding surface $\sigma = 0$ with a width of 1 deg.

Figure 11 presents the interceptor and target trajectories in the planar (X, Y) Cartesian inertial frame. In this sample scenario the target maneuver is 20 g and the initial conditions are $\theta(0) = 20$ deg, $\delta(0) = 20$ deg, and $r(0) = 5$ km. Despite the large initial heading error of 20 deg, the interceptor gradually approaches the target future trajectory and tracks it until it is caught up by the target. A similar example but for a scenario that starts initially as head-on, with initial conditions of $\theta(0) = 20$ deg, $\delta(0) = 155$ deg, and $r(0) = 15$ km, is plotted in Fig. 12. The engagement starts with a sharp turn until the HP conditions are reached.

In Figs. 13–18 the interceptor relative trajectories, sliding surface value, and missile acceleration profiles are plotted for $\theta_r = 0$ deg, 10 deg. The initial conditions for the scenario investigated are $\theta(0) = 20$ deg, $\delta(0) = 20$ deg, and $r(0) = 5$ km. In each figure three different trajectories are plotted, corresponding to target maneuvers of −20, 0, and 20 g.

From Figs. 13 and 14 it can be seen that, even in the presence of target maneuvers and initial heading errors, interception is achieved

Table 1 Simulation parameters

Missile	Target	Guidance
$V_I = 1600$ m/s $\tau_I = 0.2$ s	$V_T = 2000$ m/s $a_T \in \{-20\text{ g}, 0\text{ g}, 20\text{ g}\}$ $\tau_T = 0.2$ s	$n = 3$ $\tau = 0.1$ s

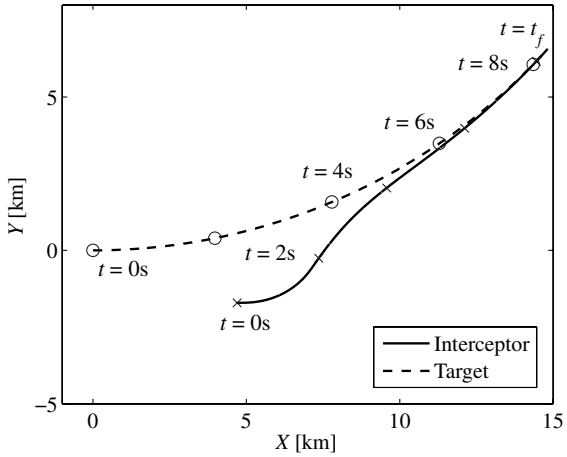

Fig. 11 Sample HP inertial trajectories; $a_T = 20$ g, $\theta(0) = 20$ deg, $\delta(0) = 20$ deg, $r(0) = 5$ km.

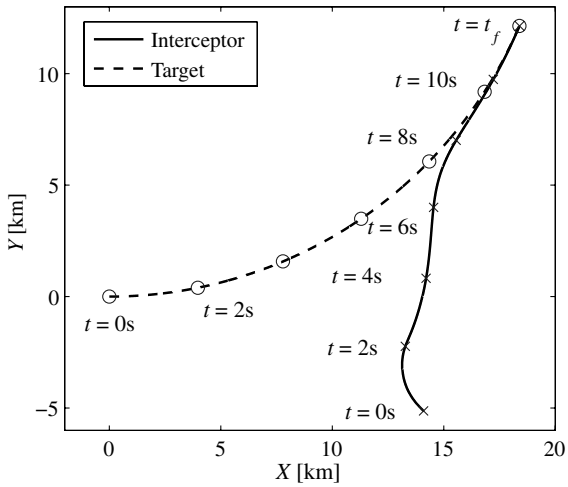

Fig. 12 Sample HP inertial trajectories initiated as head-on; $a_T = 20$ g, $\theta(0) = 20$ deg, $\delta(0) = 155$ deg, $r(0) = 15$ km.

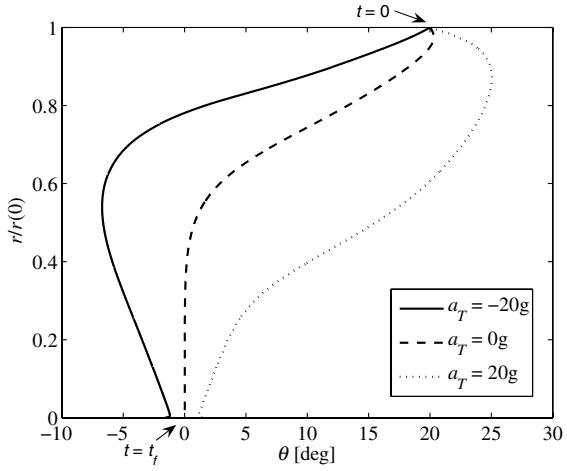

Fig. 13 Trajectories in target coordinate system; $\theta_r = 0$.

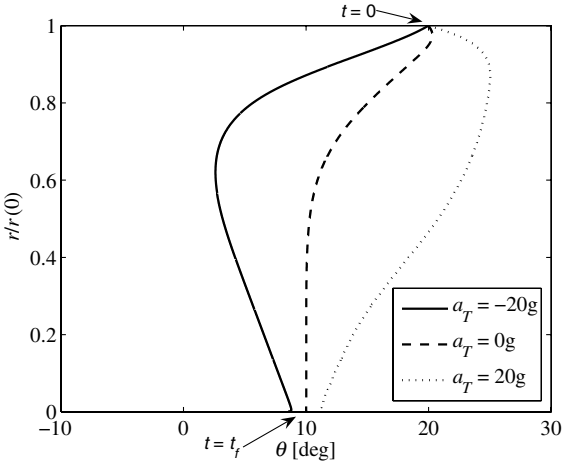

Fig. 14 Trajectories in target coordinate system; $\theta_r = 10$ deg.

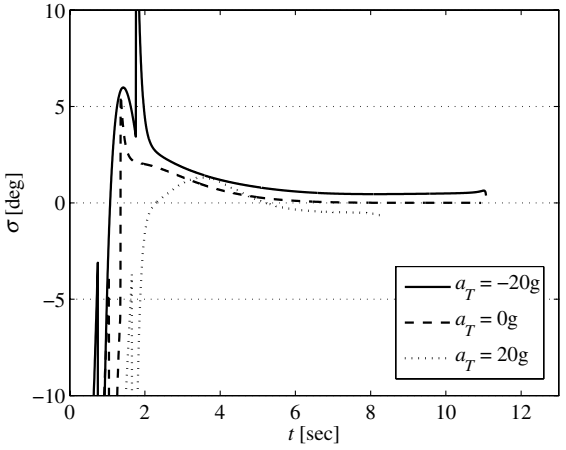

Fig. 15 Sliding variable value for different target maneuvers; $\theta_r = 0$.

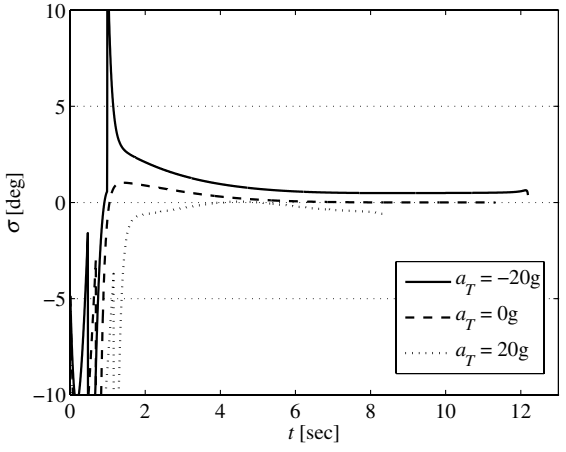

Fig. 16 Sliding variable value for different target maneuvers; $\theta_r = 10$ deg.

with θ that is close to the required one. The difference, of up to 1 deg, is due to the boundary-layer implementation of the controller. The value of the sliding variable for $\theta_r = 0$ deg, 10 deg is shown in Figs. 15 and 16, respectively. After a short transient, σ is kept within the boundary layer up to the intercept point. The difference in the scenario duration, due to the different interception geometries, is also evident. The profile of the missile acceleration in these scenarios is plotted in Figs. 17 and 18. We have implemented the guidance law with a bound of 100 g on the control. Thus, when this bound is reached early on due to the heading error, the system cannot be confined to the sliding surface. As is evident after the initial error is nullified the acceleration reaches a constant value. Note that due to its lower speed the interceptor's final maneuver, needed to maintain a trajectory with the curvature as that of the target, is smaller than the target's by a factor of $1/K^2$.

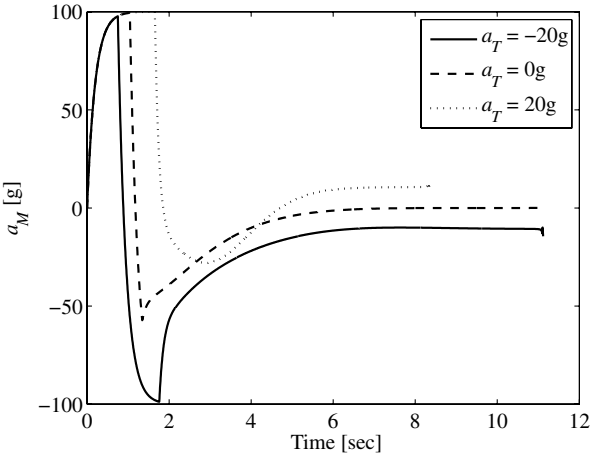

Fig. 17 Missile acceleration profile for different target maneuvers; $\theta_r = 0$.

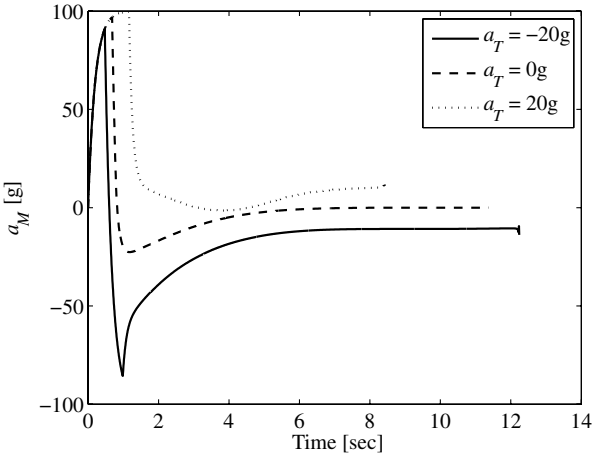

Fig. 18 Missile acceleration profile for different target maneuvers; $\theta_r = 10$ deg.

VI. Conclusions

A novel head pursuit guidance engagement was presented, in which an interceptor is placed ahead of a faster target, and both fly in the same direction. Using this approach the closing speed is significantly reduced relative to a head-on engagement; and compared to a tail-chase engagement, the low closing speed can be achieved with reduced energy requirement.

The new proposed head pursuit guidance law is based on enforcing the required geometric relation of intercepting the target from its front. It also enables enforcing the interception from a predetermined angle relative to the target's flight trajectory.

A sliding mode approach was proposed for implementing the guidance law. The controller allows bringing the system to a sliding surface that imposes the required geometric rule. Simulation results confirmed that this surface can be reached and maintained in face of target maneuvers and large initial heading errors.

Acknowledgment

The work of Tal Shima was supported in part by a Horev Fellowship, through the Taub Foundation, at the Technion.

References

[1] Golan, O. M., Rom, H., and Yehezkely, O., "System for Destroying Ballistic Missiles," U.S. Patent No. 6,209,820 B1, 3 April 2001.

[2] Zes, D., "Exo-Atmospheric Intercept Using Modified Proportional Guidance with Gravity Correction for Coast Phase," AIAA Paper 94-0209, 1994.

[3] Yuan, L. C., "Homing and Navigational Courses of Automatic Target Seeking Devices," *Journal of Applied Physics*, Vol. 19, Dec. 1948, pp. 1122–1128.

[4] Alfano, S., and Fosha, C. E., Jr., "Hypervelocity Orbital Intercept Guidance Using Certainty Control," *Journal of Guidance, Control, and Dynamics*, Vol. 14, No. 3, 1991, pp. 574–580.

[5] Hough, M. E., "Optimal Guidance and Nonlinear Estimation for Interception of Decelerating Targets," *Journal of Guidance, Control, and Dynamics*, Vol. 18, No. 2, 1995, pp. 316–324.

[6] Shima, T., and Shinar, J., "Time Varying Pursuit Evasion Game Models with Bounded Controls," *Journal of Guidance, Control, and Dynamics*, Vol. 25, No. 3, 2002, pp. 425–432.

[7] Shneydor, N. A., *Missile Guidance and Pursuit—Kinematics, Dynamics and Control*, Series in Engineering Science, Horwood Publishing, Chichester, U.K., 1998, Chap. 3.

[8] Bruckstein, A. M., "Why the Ants Trails Look So Straight and Nice," *The Mathematical Intelligencer*, Vol. 15, No. 2, 1993, pp. 59–62.

[9] Manchester, I., and Savkin, A. V., "Circular Navigation Missile Guidance with Incomplete Information and Uncertain Autopilot Model," *Proceeding of the AIAA Guidance, Navigation, and Control Conference*, CP-5448, AIAA, Washington, DC, 2003.

[10] Idan, M., Golan, O., and Guelman, M., "Optimal Planar Guidance Laws with Terminal Constraints," *Journal of Guidance, Control, and Dynamics*, Vol. 18, No. 6, 1995, pp. 1273–1279.

[11] Golan, O. M., and Shima, T., "Head Pursuit Guidance for Hypervelocity Interception," *Proceeding of the AIAA Guidance, Navigation, and Control Conference*, CP-4885, AIAA, Washington, DC, 2004.

[12] Slotine, J.-J. E., and Li, W., *Applied Nonlinear Control*, Prentice–Hall, Upper Saddle River, NJ, 1991, pp. 276–307, Chap. 7.

[13] Utkin, V. I., *Sliding Modes in Control and Optimization*, Springer–Verlag, Berlin, 1992.

[14] Khalil, H. K., *Nonlinear Systems*, 3rd ed., Prentice–Hall, Upper Saddle River, NJ, 2002, Chap. 13.

[15] Moon, J., and Kim, Y., "Design of Missile Guidance Law Via Variable Structure Control," *Journal of Guidance, Control, and Dynamics*, Vol. 24, No. 6, 2001, pp. 659–664.

[16] Xu, W., Mu, C., and Zhou, D., "Adaptive Sliding-Mode Guidance of a Homing Missile," *Journal of Guidance, Control, and Dynamics*, Vol. 22, No. 4, 1999, pp. 589–594.